



# Development of Maghemite Nanoparticles to Effectively Adsorb Methylene Blue Dye from Water

Muhammad Azeem Ashraf ·  
Mumtaz Hasan Malik · Assad Farooq ·  
Muhammad Tayyab Noman · Nayab Khan

Received: 4 July 2023 / Accepted: 21 March 2024 / Published online: 5 April 2024  
© The Author(s), under exclusive licence to Springer Nature Switzerland AG 2024

**Abstract** Textile dyes have a major issue of the contamination of water and are hazardous to aquatic environments. This work reports the development of an efficient process for iron oxide nanoparticle synthesis by a modified co-precipitation technique. The ultrasonic energy was used to enhance the synthesis of maghemite nanoparticles. A comprehensive study of vital process factors was carried out to develop the optimum conditions for synthesising pure Fe<sub>2</sub>O<sub>3</sub> nanoparticles. The effect of process variables was modelled and analysed with Box–Behnken statistical design and response surface methodology using Design-Expert software. The best outcome with 25-nm size was achieved with optimum processing conditions at a pH level of 12, a temperature of 70 °C, and a time of 60 min. The end products were confirmed with X-ray diffraction. Further, the nanoparticles were characterised with a scanning electron

microscope, BET, UV–visible spectrophotometer, and vibrating sample magnetometer. The method described here offers significant advantages over other techniques for the large-scale production of Fe<sub>2</sub>O<sub>3</sub> nanoparticles in a short time compared to other procedures. The prepared maghemite nanoparticles were successfully employed for methylene blue (MB) dye adsorption from water. Further, different adsorption process parameters were examined thoroughly. The data was analysed using Langmuir and Freundlich isotherms, whereas the adsorption kinetics of dye were investigated by employing the pseudo-first- and pseudo-second-order models. Higher values of R<sup>2</sup> showed better fitness of the experimental data on dye removal to the Freundlich isotherm model and pseudo-second-order kinetic model. The maximum adsorption capacity of maghemite nanoparticles was observed to be 96.52 mg g<sup>-1</sup>. The adsorbent maghemite nanoparticles can be easily restored and reused. The combination of facile desorption and effective regeneration positions the prepared maghemite nanoparticles as a compelling candidate for industrial wastewater treatment applications.

---

M. A. Ashraf · M. H. Malik  
School of Design and Textiles, University of Management  
and Technology, Lahore, Pakistan

M. A. Ashraf · A. Farooq · N. Khan (✉)  
Department of Fibre and Textile Technology, University  
of Agriculture, Faisalabad, Pakistan  
e-mail: nayab.khan@uaf.edu.pk

M. T. Noman  
Department of Machinery Construction, Institute  
for Nanomaterials, Advanced Technologies  
and Innovation, Technical University of Liberec, Liberec,  
Czech Republic

**Keywords** Iron oxide nanoparticles · Maghemite ·  
Adsorption · Dye removal · Wastewater

## 1 Introduction

The impact of environmental issues on health has drawn attention from all across the world. Exposure to environmental pollution results in many human diseases. Inappropriate handling and disposal of industrial waste is the leading cause of environmental deterioration. According to World Bank estimates, textile wet processing treatments are responsible for 17–20% of water pollution (Zhou et al., 2010).

Colours are broadly utilised in numerous modern fields, for example, materials, plastics, textiles, and paper. It has been estimated that 10–15% of the colouring materials were wasted during the colouration of materials and discharged as waste (Al-Ghouti et al., 2003). The release of non-degradable synthetic colouring materials into water has caused worldwide concern due to ecological problems. These colours are mainly hard to degrade due to their intricate structure. The existence of these colours in wastewater is highly objectionable, even in meagre amounts. Many dyes are considered harmful and cancer-causing for humans and animals (Uddin et al., 2009). Therefore, the advancement of new methods to reduce the release of dyes into water is of extraordinary significance.

Several studies have been conducted for the elimination of colour from water through many techniques, such as adsorption (Mahanta et al., 2008; Rachiq et al., 2021), membrane filtration (Lee et al., 2006; Loukili et al., 2008), coagulation (Anouzla et al., 2009; Shi et al., 2007), and photocatalysis (Azarang et al., 2014, 2015; Fernandez et al., 2002; Moussadik et al., 2023; Yousefi et al., 2015). The importance of adsorption is significantly higher among all the techniques mentioned above as it provides high productivity, is easy-to-handle operation, and is more effective than other relevant methods. Different adsorbents, including polymeric materials (Yu et al., 2003), composite electro spun fibres (Zhao et al., 2017a, 2017b; Zhao et al., 2015), zeolites (Lee et al., 2007), clays (Espantaleon et al., 2003; Loukilia et al., 2021), and activated carbons (Al-Degs et al., 2000), have been exploited for the elimination of dyes from water. However, these materials have many shortcomings, such as low adsorption power and difficult recovery from the solution. Hence, new adsorbents with high adsorption power and easy recovery from the solution are essential in wastewater treatment.

Due to their attractive properties, iron-containing nanoparticles are being employed in several fields, such as medical treatment and diagnosis, magnetic storage devices, catalysis, environmental remediation processes, and sensors. The central fact behind the much attention focused on producing and characterising iron-containing nanoparticles is their extraordinary properties compared with their bulk material. Iron oxide nanoparticles with a superparamagnetic nature are mainly used in medicinal sciences, magnetic resonance imaging (MRI), and biosensors (Raming et al., 2002; Zhong et al., 2006).

For synthesising homogeneous iron oxide nanomaterials, many methods have been utilised, like co-precipitation, thermal decomposition, hydrothermal, sol–gel, and precursor (Cao et al., 2005; Chauhan et al., 1999; Ganguli & Ahmad, 2007; Hyeon et al., 2001; Morello III et al., 2007; Rockenberger et al., 1999; Sonavane et al., 2007). However, most of the described methods have some drawbacks, such as (i) difficult-to-handle reagents, (ii) metal complex precursors which are usually expensive and difficult to prepare, (iii) strong acids or alkalis, (iv) costly instruments, and (v) formation of undesired products (Mendoza et al., 2005). Therefore, developing a facile process to prepare iron oxide nanoparticles of the desired phase is still challenging. This research work was carried out to address the shortcomings of conventional methods.

The most commonly used technique to manufacture iron oxide ( $\text{Fe}_3\text{O}_4$  and  $\gamma\text{-Fe}_2\text{O}_3$ ) nanoparticles is the co-precipitation technique through which ferric and ferrous ions are reacted at higher temperatures in an alkaline medium. The geometry of  $\text{Fe}_2\text{O}_3$  NPs produced is influenced mainly by the ferrous and ferric ion ratios, the type of salt used in the production, the medium's pH, the reaction's temperature, and many other process variables like stirring and the addition rate of chemicals (Wu et al., 2008). This method has a critical influence on the synthesised  $\text{Fe}_2\text{O}_3$  NPs. The saturation magnetisation values of nanomaterials are mainly observed to be smaller than their bulk-size materials (Binh et al., 1998).

The ultrasonic-assisted approach is an economical process for the production of nanomaterials. Compared to any other technique, this method is superior to all others in terms of its ability to regulate the size and crystallinity of the end product. This is due to the fact that, through the propagation of sound waves, the

material undergoes physical and chemical changes as a result of ultrasonic energy. These waves cause a great number of bubbles, which ultimately explode to produce excessive heat energy, which can significantly increase the local temperature and pressure (Guo et al., 2011). The ultrasonic-assisted method has been used by many scientists for nanomaterial synthesis (Gedanken, 2004; Ghows & Entezari, 2010; Nguyen et al., 2023; Patil & Pandit, 2007; Zhang et al., 2023).

This work reports the ultrasonic-assisted synthesis of maghemite in pure form with a modified co-precipitation method. A comprehensive study of essential process variables such as pH of the medium, temperature of the reaction, and duration of the reaction process was done to develop the optimum process for synthesising pure iron oxide nanoparticles. The end products were confirmed with X-ray diffraction. Further, the synthesised nanoparticles were characterised with a scanning electron microscope (SEM), spectrophotometer, and vibrating sample magnetometer (VSM). The synthesised nanoparticles were employed for the adsorption of MB dye from the solution. The thermodynamics and adsorption kinetics of MB on maghemite nanoparticles were studied using various models. The main benefits of this procedure are that the process is quite simple, and raw materials used to synthesise nanoparticles are nontoxic and environmentally friendly. Also, this method does not need any complex purification or separation procedures, so the maghemite nanoparticles could be synthesised in a single step. Further, the synthesised nanoparticles can be easily recycled and reused for the elimination of dyes from the solution.

The objectives of this research work are to optimise the synthesis of maghemite nanoparticles by ultrasonic-assisted method to achieve the minimum size and efficient adsorption of dyes from water with synthesised nano-adsorbent. The experiments were planned with Box–Behnken statistical design. The results were analysed with response surface methodology using Design-Expert software.

## 2 Experimental

### 2.1 Materials

Chemical reagents, i.e. Fe(III) chloride hexahydrate, iron(II) sulphate heptahydrate, ammonium hydroxide,

sodium hydroxide, hydrochloric acid, nitric acid, and methylene blue (MB) dye, were procured from Sigma Aldrich. The calibration spectra of MB were measured by spectrophotometer (Datacolor 850 Spectrophotometer, Datacolor, USA) to verify the actual concentration of dye in the prepared solutions.

### 2.2 Synthesis

The synthesis of maghemite nanoparticles was carried out with ultrasonic-assisted modified co-precipitation method. A mixture of ferrous sulphate heptahydrate (6.08 g, 200 mM) and ferric chloride hexahydrate (21.62 g, 400 mM) at a stoichiometric ratio of 1:2 was prepared in 200 mL of water. The whole solution was placed in an ultrasonic bath. A few drops of HCl were added to stabilise the anionic surface charges. Then, NH<sub>4</sub>OH was used dropwise to achieve the desired pH, resulting in the formation of a black precipitate. The process of synthesis was carried out at specific temperatures and times according to the experimental plan as given in Table 1 and Table 2. Then, 100-mL nitric acid was added for the oxidation of iron oxide. The precipitate turned dark brown, showing the formation of maghemite. Deionised water was used to wash the obtained nanoparticles. The resultant nanoparticles were separated with a magnet and dried.

### 2.3 Design of Experiment

Box–Behnken design is the most widely used statistical design in the response surface methodology for process modelling and optimisation (Abrouki et al., 2021). Box–Behnken statistical design with a central point (0) and factorial points ( $\pm 1$ ) was used for this research work. Box–Behnken design with three different input variables (pH, temperature, and time), their assigned symbols, and ranges

**Table 1** Selected factors with their levels for the synthesis of iron oxide nanomaterials

Factors	Range levels		
	− 1	0	+ 1
pH	8	10	12
Temperature (°C)	30	50	70
Time (min)	30	60	90

**Table 2** Design of the experiment and resultant size of the maghemite nanoparticles

Sample no	A: pH	B: temperature (°C)	C: time (min)	Nanoparticle size (nm)	
				Experimental	Predicted
1	12	50	30	49	49.75
2	8	50	30	53	52.50
3	12	30	60	45	42.13
4	12	50	90	65	65.50
5	10	50	60	39	40.00
6	10	50	60	40	40.00
7	10	70	90	74	71.88
8	10	30	90	70	72.38
9	10	50	60	41	40.00
10	10	50	60	38	40.00
11	10	70	30	40	37.63
12	12	70	60	25	26.63
13	8	70	60	34	36.87
14	8	30	60	50	48.37
15	10	50	60	42	40.00
16	8	50	90	80	79.25
17	10	30	30	62	64.13

is displayed in Table 1. The analysis of variance (ANOVA) test was utilised to evaluate the linear and quadratic effects of each variable and their interactions with the output response. A 95% confidence interval ( $p$ -value < 0.05) was taken into account. After the ANOVA test, the behaviour of input and output factors was evaluated by using response surface methodology (RSM). This method is useful for assessing response surfaces via quadratic model fitting (Anouzla et al., 2022). Design-Expert software by Stat-Ease Corporation was used for designing experiments and optimisation of independent factors. The experimental setup with different pH conditions, temperature, and time based on the Box–Behnken design along with the results of nanoparticle size is presented in Table 2. The quadratic Eq.(1) was used to adjust the impact of variables on results.

$$Y = b_0 + \sum b_i X_i + \sum b_{ij} X_i X_j + \sum b_{ii} X_i^2 \quad i \geq j, j = 1, 2, 3 \quad (1)$$

where  $b_0$  represents the coefficient of the constant term in the equation, the coefficient  $b_i$  of the linear term describes the influence of the variables, the coefficient of the quadratic term is denoted by  $b_{ii}$ , and the two-factor interaction coefficient is represented by  $b_{ij}$  (Noman et al., 2019).

## 2.4 Characterisation

To comprehend the system underlying the elimination of contaminants from water using adsorbents, it is imperious to investigate the adsorbents for different surface features (Imran et al., 2020; Iqbal et al., 2019; Naeem et al., 2019). The surface characteristics of the nanoparticles were measured with UHR FE-SEM (Carl Zeiss Meditec AG, Jena, Germany). PANalytical X-ray diffractometer (Netherlands) equipped with a scintillator detector was used to measure XRD patterns to detect the structure of prepared nanoparticles. The nanoparticle surface area was analysed with the help of the Autosorb iQ instrument from Anton Paar GmbH by the Brunauer–Emmett–Teller (BET) method. The UV–visible spectra of samples were acquired with a spectrophotometer (Datacolor 850 Spectrophotometer, Datacolor, USA). VSM (Lake Shore 7407) was employed to observe the magnetic characteristics of as-prepared nanoparticles.

## 2.5 Adsorption Experiments

Different trials were conducted to analyse the MB dye adsorption on maghemite nanoparticles. For the determination of optimum conditions for removal of MB by maghemite nanoparticles, experimental

parameters were dye initial concentration (5 to 25 mg L<sup>-1</sup>), adsorbent dosage (4 to 20 mg L<sup>-1</sup>), pH (2 to 10), temperature (25 to 45 °C), and agitation speed (0 to 200 rpm). The solutions' pH was maintained with HCl (0.1 mol L<sup>-1</sup>) or NaOH (0.1 mol L<sup>-1</sup>) solutions.

The proportion of the MB dye removal from solutions is measured with Eq. (2).

$$R(\%) = \frac{(C_o - C_t)}{C_o} \times 100 \quad (2)$$

In Eq. (3), adsorption capacity at any given time  $t$  was determined.

$$q_t = \frac{(C_o - C_t)V}{m} \quad (3)$$

In the above equation,  $C_o$  (mg L<sup>-1</sup>) expresses the initial dye concentration, while at any given time  $t$  (min),  $C_t$  (mg L<sup>-1</sup>) represents dye concentration, whereas  $m$  (g) represents the mass of nano-adsorbent and  $V$  (L) denotes the volume of solution.

---


$$\begin{aligned} \text{Nanoparticlesize} = & 117.6 + 5.06(\text{pH}) - 0.52(\text{temperature}) - 2.71(\text{time}) - 0.03(\text{pH} \times \text{temperature}) \\ & - 0.05(\text{pH} \times \text{time}) + 0.01(\text{temperature} \times \text{time}) - 0.16 \times (\text{pH})^2 \\ & - 0.002(\text{temperature})^2 + (\text{time})^2 \end{aligned} \quad (4)$$


---

The effect of selected factors on the outcomes is statistically evaluated by the ANOVA test. The results demonstrate the statistical significance of the established model for particle size at  $p$ -value < 0.0001 and  $F$ -value 53.78 as mentioned in Table 3. The statistical analysis shows that there is a 0.01% chance that an  $F$ -value of this magnitude could be caused by noise. The capability of the established model is acceptable, as  $p$ -values < 0.05 show the importance of the model terms. Therefore, the model terms A, B, C, BC, and C<sup>2</sup> are significant. However, the model terms AB, AC, A<sup>2</sup>, and B<sup>2</sup> showed non-significant effects.

$$R^2 = 0.9857, \text{ adjusted } R^2 = 0.9674.$$

The use of three-dimensional diagrams is an effective method for gaining a deeper understanding of the impact of various factors and for analysing their interrelationships. Response surface plots are

### 3 Results and Discussion

The results of this work are presented here.

#### 3.1 Size of the Nanoparticles

The measured size of the resultant maghemite nanoparticles in response to different processing conditions is presented in Table 2. For this study, a total of 17 samples were prepared with variations in pH, temperature, and time. The results indicate that the nanoparticles' size increased after a certain time interval. The findings revealed an enhancement in the particle size from 34 to 80 nm, 45 to 70 nm, and 40 to 62 nm by varying the individual variables from their minimum to maximum levels. However, the best outcome with a 25-nm size was achieved for sample number 12 with optimum processing conditions at a pH level of 12, a temperature of 70 °C, and a time of 60 min.

A mathematical model was designed for the analysis and prediction of the size of nanoparticles as presented in Eq. (4). This model can predict the result at any given point in space.

utilised to demonstrate how inputs affect the final nanoparticles' particle size. These plots are helpful for the visualisation of input variables' effect on output responses. The interaction results for the influence of essential process variables on the synthesis of maghemite nanoparticles are presented in Fig. 1.

According to the process modelling and experimental results, the process for the synthesis of nanoparticles was optimised to achieve the minimum size of the nanoparticles using Design-Expert software version 13. Among the available 100 solutions, the first solution was chosen with a desirability of 1.000 as presented in Fig. 2. Therefore, the optimum settings for the synthesis of maghemite nanoparticles were chosen as follows: pH level of 12, a temperature of 70 °C, and a time of 60 min.

**Table 3** Analysis of variance (ANOVA) results regarding the size of nanoparticles

Source	Sum of squares	df	Mean square	F-value	p-value	
Model	3716.72	9	412.97	53.78	<0.0001	Significant
A—pH	136.12	1	136.12	17.73	0.0040	
B—temperature	364.50	1	364.50	47.47	0.0002	
C—time	903.13	1	903.13	117.62	<0.0001	
AB	4.00	1	4.00	0.5209	0.4938	
AC	30.25	1	30.25	3.94	0.0876	
BC	169.00	1	169.00	22.01	0.0022	
A <sup>2</sup>	1.64	1	1.64	0.2142	0.6575	
B <sup>2</sup>	3.22	1	3.22	0.4198	0.5377	
C <sup>2</sup>	2107.96	1	2107.96	274.53	<0.0001	
Residual	53.75	7	7.68			
Lack of fit	43.75	3	14.58	5.83	0.0607	Not significant
Pure error	10.00	4	2.50			
Cor total	3770.47	16				

**Fig. 1** The 3D response surfaces and contour plots for nanoparticle size under the effect of **a** pH, temperature; **b** pH, time; and **c** temperature, time

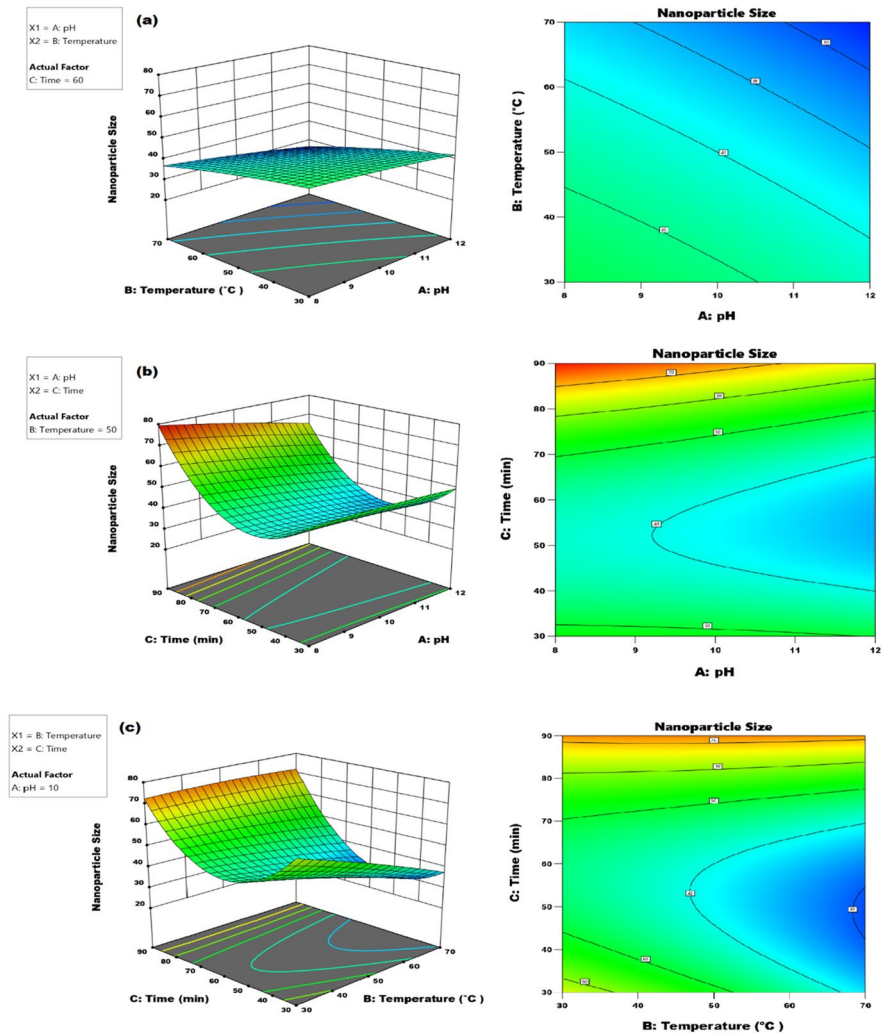


**Fig. 2** Optimisation ramps for the process factors to achieve the minimum size of nanoparticles

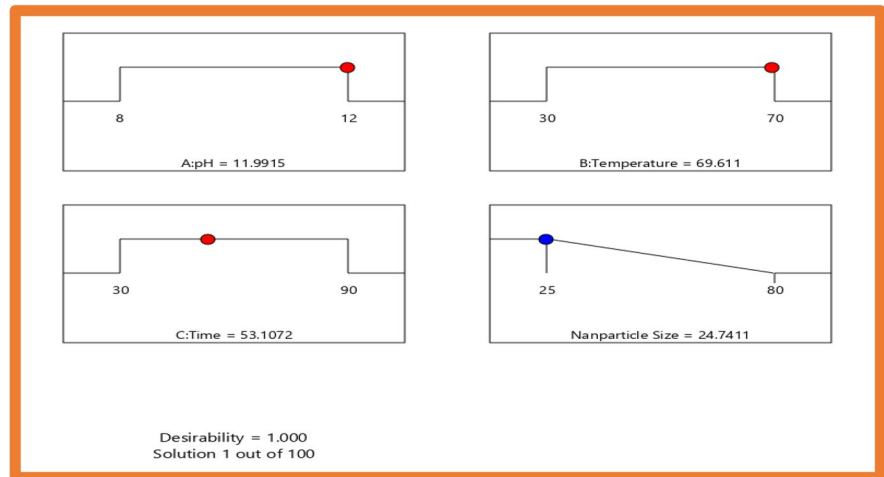
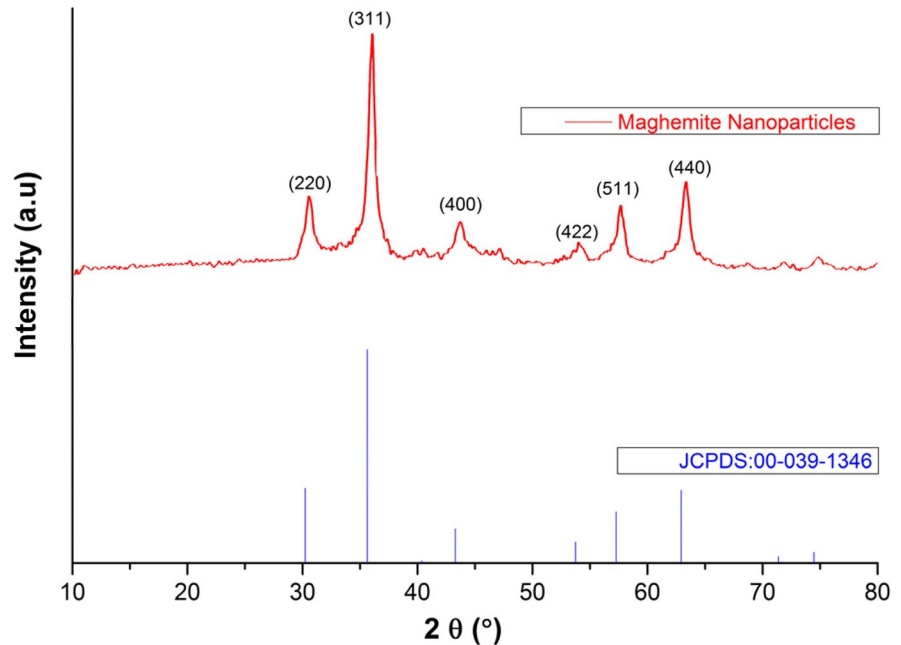


**Fig. 3** XRD patterns of maghemite nanoparticles



### 3.2 XRD Analysis

The XRD spectra of as-synthesised maghemite nanoparticles are presented in Fig. 3.

The obtained peaks, i.e. 220, 311, 400, 422, 511, and 440 of the XRD diffraction pattern, represent the cubic spinel structure of the powder diffraction database with a card no. (JCPDS No. 39–1346) as shown in Fig. 3. These patterns confirm the pure crystals of maghemite iron oxide nanoparticles. These XRD findings are in agreement with other researchers (Guivar et al., 2014; Horner

et al., 2009; Wu et al., 2010). The XRD peak at 311 shows a strong maghemite crystalline structure of nanoparticles (Hyeon et al., 2001). The synthesised nanoparticles' average crystal size was 25 nm, as determined by the Scherer equation from the XRD study (Saravanan et al., 2013). The calculated lattice constant of prepared maghemite nanoparticles by diffraction data was  $8.3491 \pm 0.0005 \text{ \AA}$ , which is well in line with that of bulk maghemite ( $8.3505 \text{ \AA}$ ) (Goss, 1988). The d-spacing values are presented in Table 4.

**Table 4** d-Spacing of the as-synthesised maghemite nanoparticles

h k l	d-Spacing
220	2.95300
311	2.51770
400	2.08860
422	1.70450
511	1.60730
440	1.47580

### 3.3 SEM Analysis

SEM images were captured at various magnifications to observe the surface of the synthesised nanoparticles of iron oxide. The samples were prepared with a gold coating using a plasma sputtering device for SEM analysis. Micrographs of as-synthesised iron oxide nanoparticles using high-resolution SEM are displayed in Fig. 4. It is obvious that the resultant nanoparticles were extremely small and smooth, with a spherical shape predominating in most cases. The average size of maghemite nanoparticles was determined to be 25 nm at optimum processing conditions

at a pH level of 12, a temperature of 70 °C, and a time of 60 min.

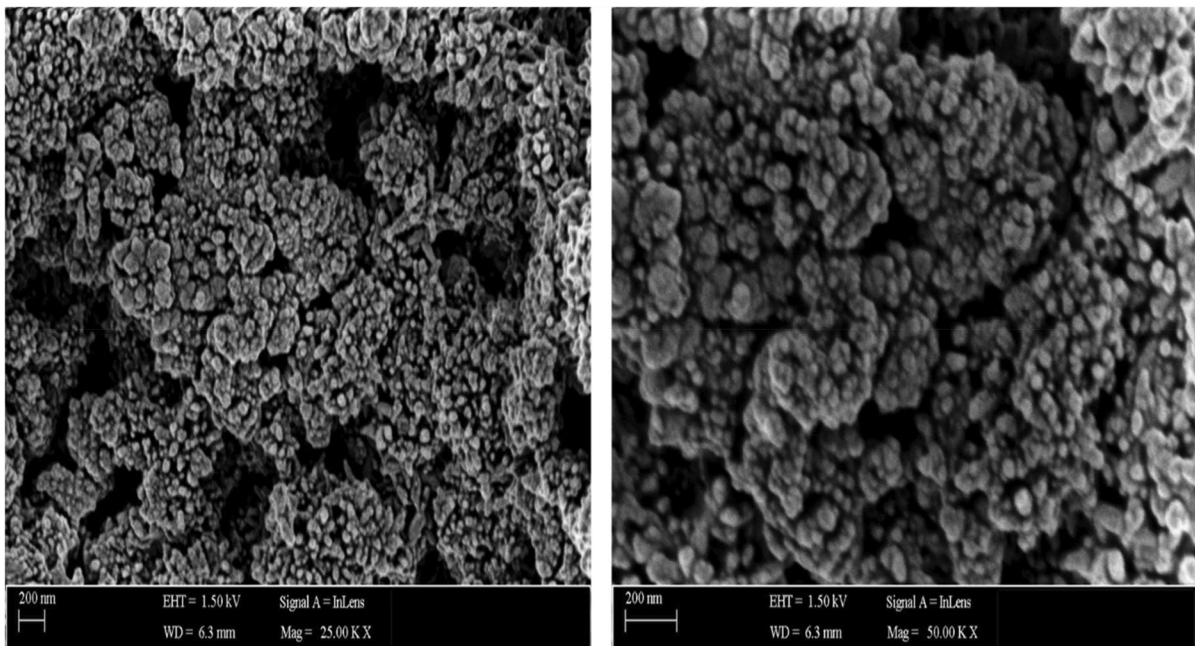
### 3.4 Surface Area Analysis

Maghemite nanoparticles' surface area was measured using N<sub>2</sub> adsorption/desorption with the BET method to assess the adsorption ability of synthesised nanoparticles. The BET plot is presented in Fig. 5. The BET technique has served as a prevailing tool for uncovering the secrets of the nanoscale world. This method is widely considered the gold standard for measuring the surface area of materials, particularly at the nanoscale. A linear BET multipoint plot of  $1/[W(P/P_0) - 1]$  vs  $P/P_0$  is presented in Fig. 5.

The surface area of maghemite nanoparticles prepared at optimum conditions (sample no. 12) was observed to be 190 m<sup>2</sup> g<sup>-1</sup>. The high surface area of iron oxide nanoparticles contributes to the significantly higher adsorption capacity of these particles.

### 3.5 Optical Properties

The synthesised nanoparticles were dispersed in water and studied for their absorption spectra at room

**Fig. 4** SEM images of iron oxide nanoparticles



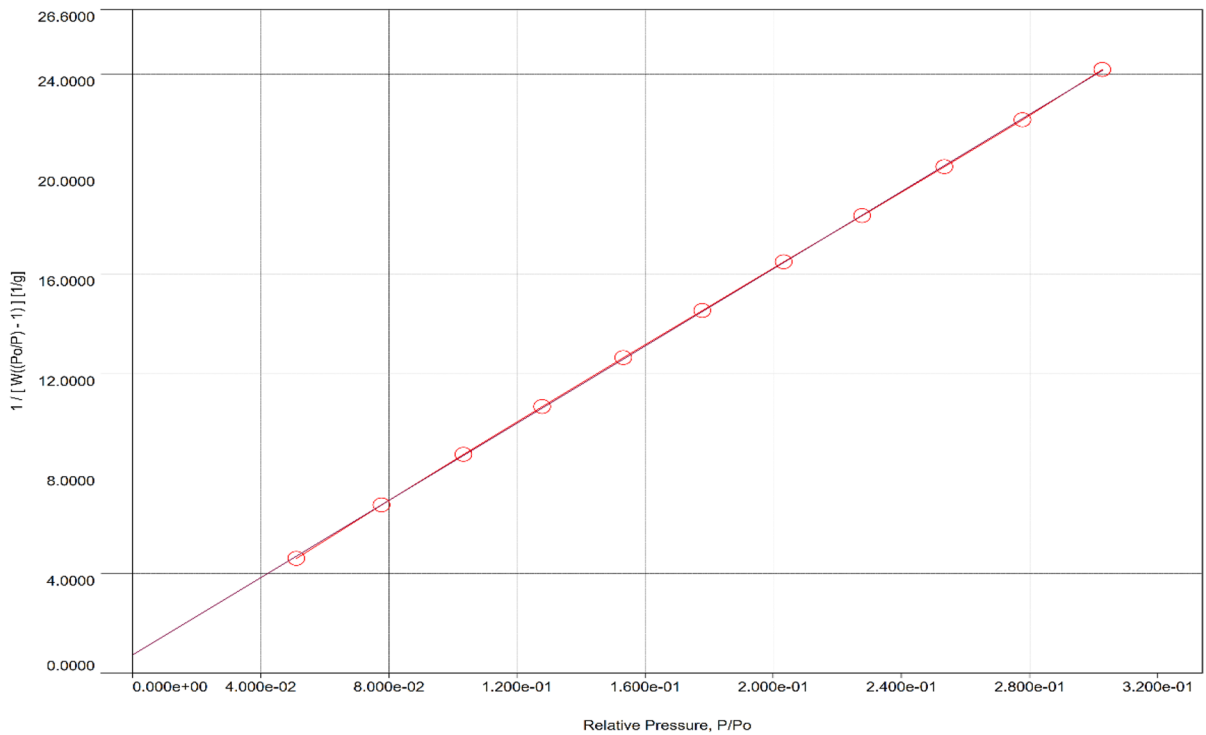
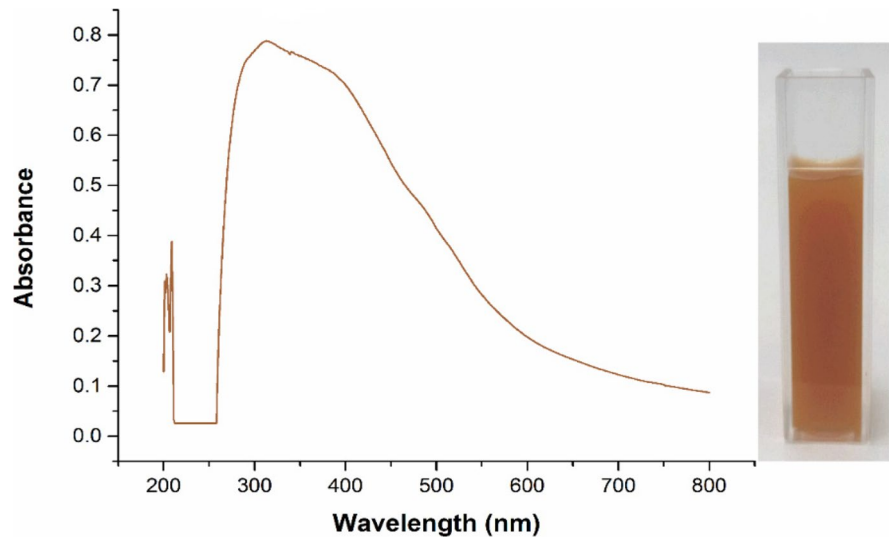


**Fig. 5** BET plot for maghemite nanoparticles

**Fig. 6 a** The absorbance spectra. **(b)** Digital image of solution of maghemite nanoparticles

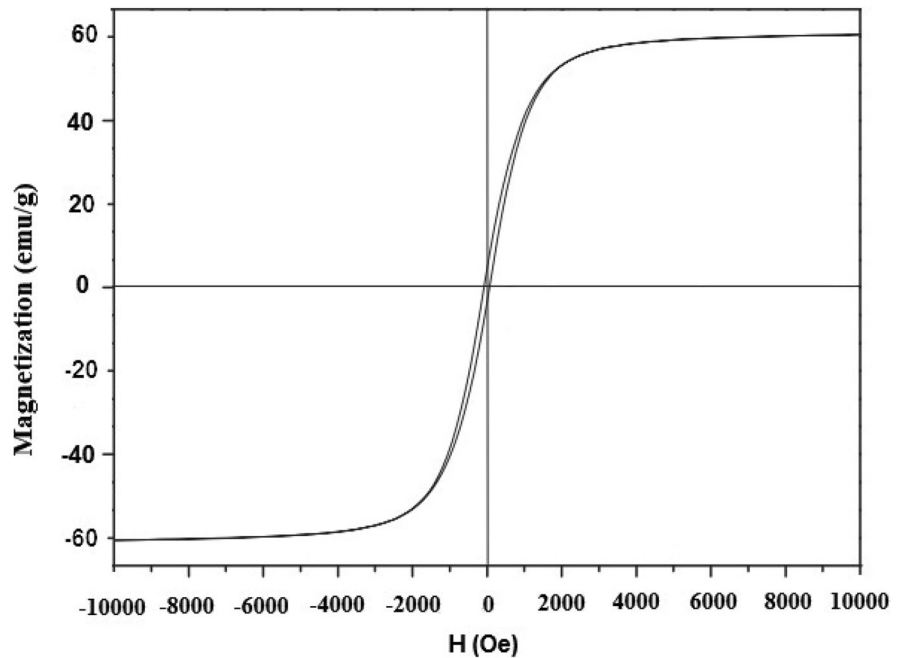


temperature. Maghemite nanoparticles demonstrated a sharp absorption peak around 315 nm, as shown in Fig. 6. It is observed that the colour of the maghemite nanoparticle solution is brownish, which also confirms the formation of maghemite.

### 3.6 Magnetic Properties

The magnetic hysteresis loop of maghemite nanoparticles is shown in Fig. 7. It was observed that the magnetic saturation of maghemite nanoparticles

**Fig. 7** Magnetisation hysteresis curves of synthesised maghemite nanoparticles



was  $61 \text{ emu g}^{-1}$  with a  $7 \text{ emu g}^{-1}$  remanent magnetisation. Maghemite nanoparticles showed typical ferromagnetic characteristics. The lower Ms of maghemite nanoparticles than their bulk may be due to surface spin effects (Morales et al., 1999), as described by other investigators (Jing, 2006; Woo et al., 2004).

The magnetic properties of ferromagnetic material were considered to rely on the materials' size, surface, and crystalline nature. Different magnetic characteristics of the developed nanoparticles are due to the surface morphology and crystal size. The higher magnetic saturation of maghemite nanoparticles may be due to shape anisotropy and magneto-static dipole interactions.

### 3.7 The Application of Maghemite Nanoparticles for the Adsorption of Methylene Blue

#### 3.7.1 Effect of MB Dye Concentration on the Adsorption

The investigation of the effects of initial concentrations of dye is important for perspective uses of the adsorbent. The starting amount of the dye determines

the saturation of the surface of the adsorbent. In the present study, at various initial dye concentrations, the quantity of dye removed by adsorption and the percent of dye adsorbed were measured under varying concentrations from  $5$  to  $25 \text{ mg L}^{-1}$  at  $25^\circ\text{C}$ , pH 8, 200-rpm agitation speed, and adsorbent dosage of  $20 \text{ mg L}^{-1}$ . Figure 8 shows that as the initial dye amount in the solution went up, the percentage of dye that was removed went down. This shows that there is a negative relationship between how much dye was in the solution at first and how much MB dye was taken out. Dye removal increases with the passage of time, as it took 90 min to reach equilibrium at the  $5 \text{ mg L}^{-1}$  initial dye concentration level, whereas 150-min time was taken for  $25 \text{ mg L}^{-1}$  dye to attain equilibrium. The relative availability of adsorption sites is higher at lower concentration levels, which enhances the dye removal in a lower time.

The enhancement in adsorption capacity by a rise in the amount of dye was due to more dye particles available during the process. The findings of adsorption capacity are shown in Fig. 9. Previous researchers (Ferrero, 2015; Giri et al., 2011; Zhang et al., 2011) also had the same findings and reported a reduction in the proportion of dye removal.

**Fig. 8** The impact of adsorption time and amount of MB on dye removal

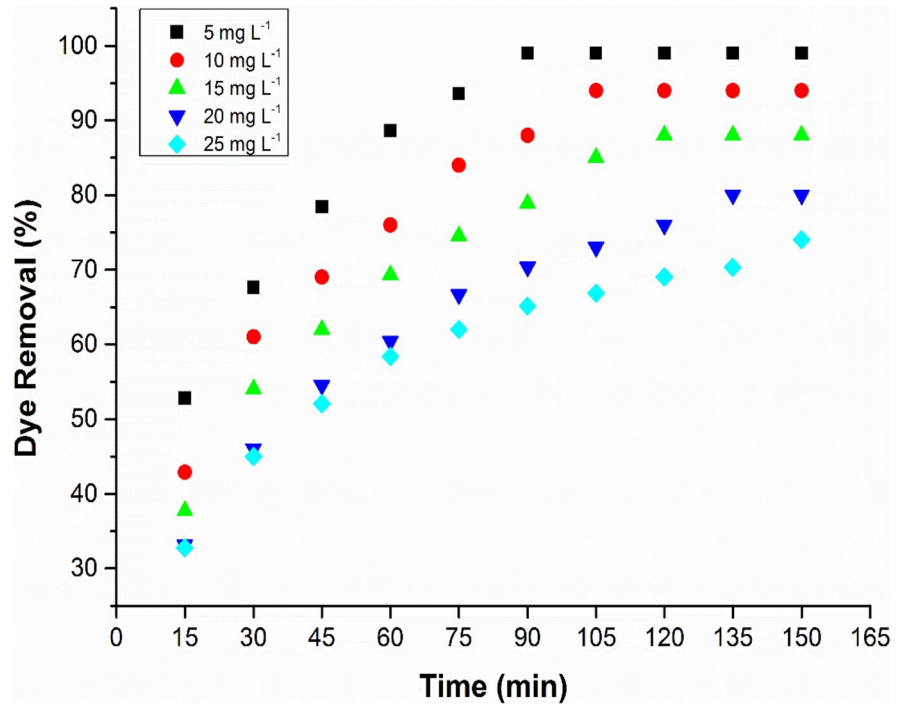
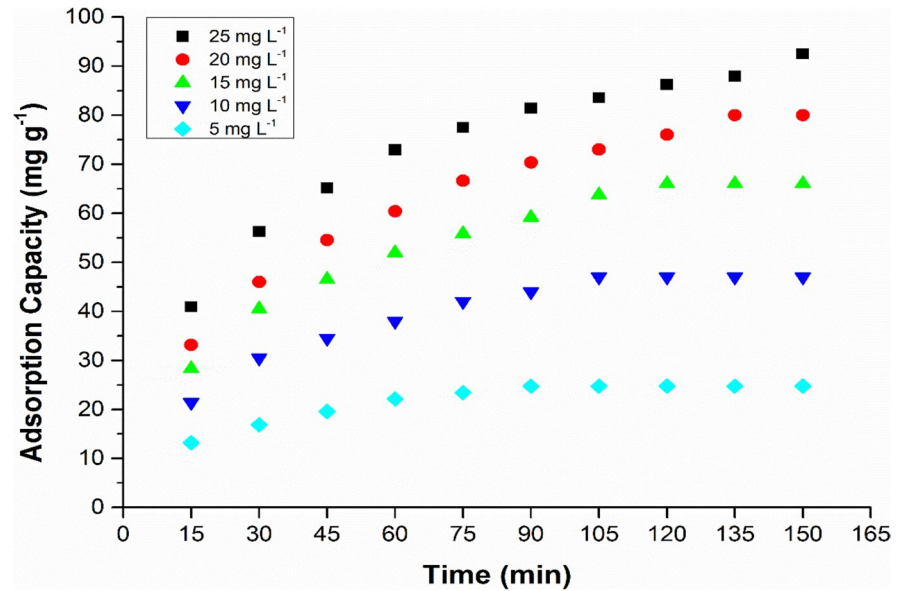


**Fig. 9** The impact of adsorption time and amount of MB on the adsorption capacity of nanoparticles

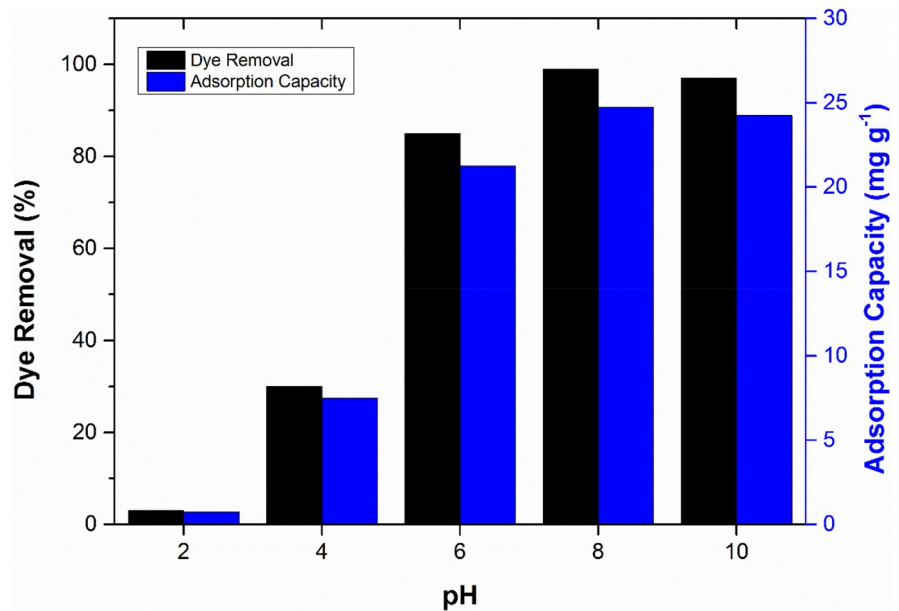


3.7.2 Effect of pH

The environment’s pH has a major impact on the functional groups of dyes. By changing the pH of the solution, dye removal has also been changed. So, the pH has a substantial impact on the kinetics of MB

adsorption by maghemite nanoparticles. Dye removal studies were conducted at various pH levels ranging from 2 to 10, and it was revealed that with an increase in the pH of the solution, both dye removal percentage and adsorption capacity increased, as presented in Fig. 10. It happens because the charge on the surface

**Fig. 10** The adsorption performance of maghemite adsorbent at different pH levels



of nanoparticles has been changed by the variation in pH level of the medium. By changing the solution's pH, the number of hydroxyl groups linked to the surface of maghemite nanoparticles varies.

At a pH of zero charge ( $pH_{pzc}$ ), there is a neutral surface charge for maghemite nanoparticles, as reported in the literature, which is around 6.6 (Garcell et al., 1998; Kosmulski, 2009; Vayssieres, 2009). Below this pH, the surface of the adsorbent is charged positively by the number of positive (H<sup>+</sup>) ions accumulated on it from the solution. Therefore, the removal of dye decreased below  $pH_{pzc}$  as the electrostatic repulsive forces increased between positive molecules of dye and the adsorbent surface of maghemite, which is also positively charged, while on the other side, a pH higher than  $pH_{pzc}$  gives a negatively charged surface to the adsorbent due to deprotonation, and dye removal increased as a result of electrostatic attractions between dye molecules of MB which have a positive charge and negatively charged surface of the maghemite adsorbent. The dye removal efficiency was highest at pH 8, so we determined that this was the best pH value to conduct adsorption experiments.

### 3.7.3 Effect of Temperature

Dye removal by maghemite nanoparticles was performed at three levels of temperature, i.e. 25 °C, 35 °C, and 45 °C, to investigate the influence of

temperature with 5 mg L<sup>-1</sup> MB initial concentration, 8 pH, 200-rpm stirring speed, and 20 mg L<sup>-1</sup> adsorbent dosage. A small decline in dye removal was detected by increasing temperature, as illustrated in Fig. 11.

### 3.7.4 Effect of the Dosage of Adsorbent

For practical uses and economic considerations, it is critical to determine the best amount of the dosage that can efficiently remove the pollutants from the water. The amount of the adsorbent material determines both the area and the quantity of sites that are accessible for adsorption (Iqbal et al., 2019). The investigations to study the effect of the adsorbent dosage were performed with a 200-rpm stirring speed, 5 mg L<sup>-1</sup> MB initial concentration, pH 8, and 4–20 mg L<sup>-1</sup> adsorbent amount. It is experienced that the degree of dye removal is enhanced by increasing the dosage of the adsorbent due to increased adsorption sites, but on the other side, adsorption capacity decreased progressively, as shown in Fig. 12. Dye removal was 75% at 4 mg L<sup>-1</sup>, which increased to 99% at 20 mg L<sup>-1</sup> adsorbent dosage. Our findings were sufficiently supported by the report that an increased adsorbent dose subsequently resulted in the presence of additional active sites where contaminants can be adsorbed (Kumar & Kumaran, 2005).

**Fig. 11** Dye removal percentage by maghemite nanoparticles at different temperature levels

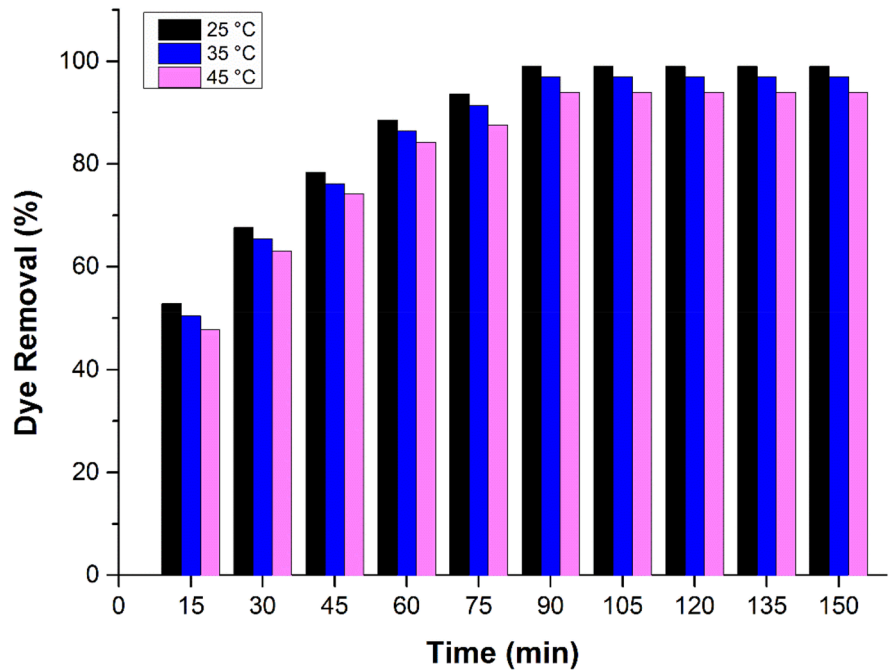
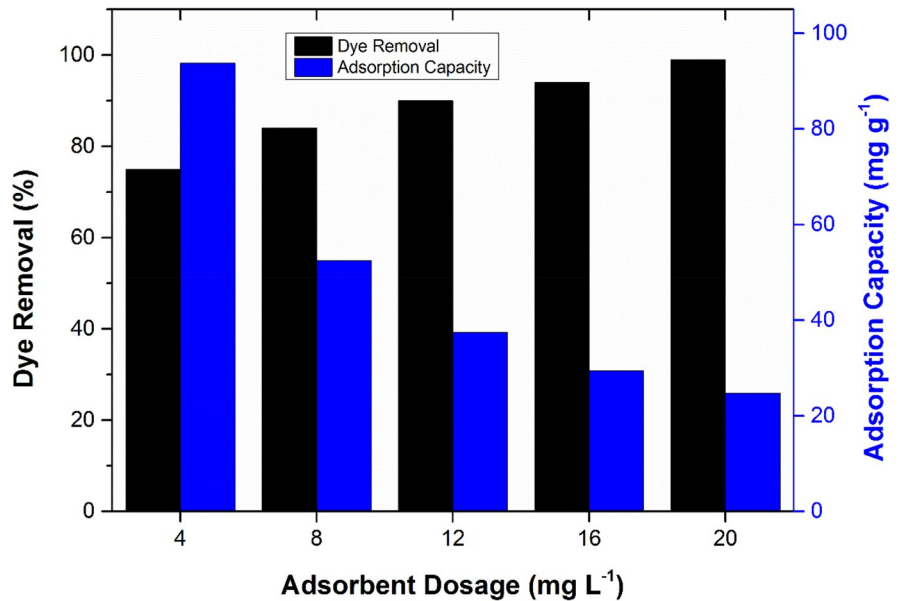


**Fig. 12** The impact of the adsorbent amount on adsorption of MB

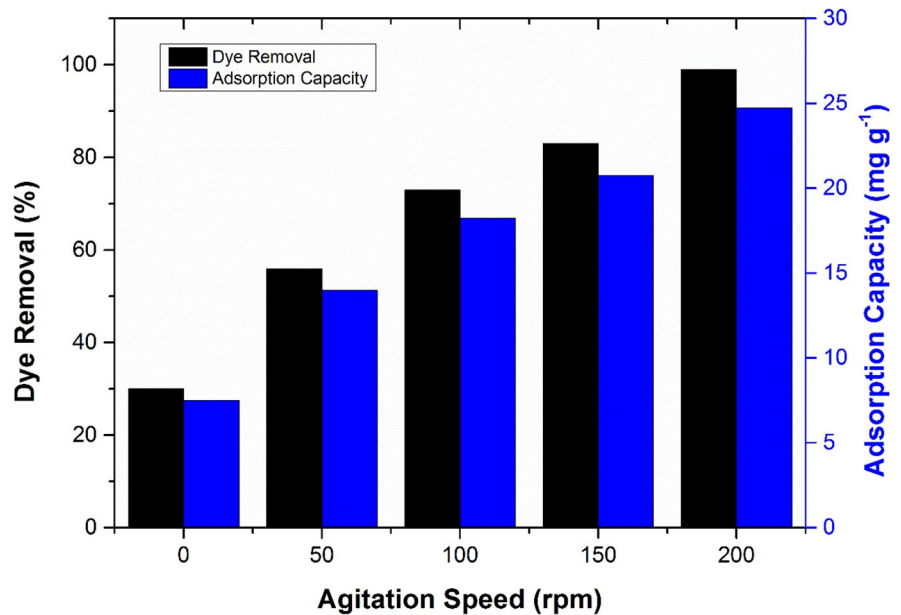


**3.7.5 Effect of Agitation Speed**

To investigate the impact of agitation speed on the adsorption of MB by maghemite nanoparticles, the following process parameters, e.g. agitation speed, initial concentration, pH, and adsorbent dosage, were varied from 50 to 200 rpm, 5 mg L<sup>-1</sup>, 8, and 20 mg

L<sup>-1</sup> respectively, and outcomes are illustrated in Fig. 13. We came to know that both dye removal percentage and adsorption capacity have been increased significantly by increasing stirring speed. This happened because as we increased the agitation speed, the interactions among adsorbent and dye molecules increased.

**Fig. 13** Impact of agitation speed on adsorption of MB



### 3.7.6 Adsorption Isotherms

Isotherms correlate the concentration of adsorbent in liquid and solid phases. The experiments were performed with 200-rpm stirring speed, 25 °C temperature, pH 8, and 20 mg L<sup>-1</sup> adsorbent amount by using various concentrations of MB dye.

The adsorption for monolayers on a homogeneous surface of adsorbent is assumed by Langmuir isotherm, which is illustrated in its nonlinear form (Langmuir, 1916) in Eq. (5).

$$q_e = \frac{q_m K_L C_e}{1 + K_L C_e} \quad (5)$$

whereas Eq. (6) explains the linear form of Langmuir isotherm.

$$\frac{C_e}{q_e} = \frac{1}{q_m K_L} + \frac{C_e}{q_m} \quad (6)$$

In these equations,  $C_e$  represents the dye concentration (mg L<sup>-1</sup>) at the equilibrium point in solution, while  $q_e$  is used for the adsorbed dye amount (mg g<sup>-1</sup>) at equilibrium,  $q_m$  expresses the maximum adsorption capacity (mg g<sup>-1</sup>), and  $K_L$  (L mg<sup>-1</sup>) is used for the Langmuir constant.

According to Freundlich isotherm, the distribution of functional groups is uneven. It assumes that

the adsorption is multilayer with interactions between adsorbate and adsorbent molecules.

Freundlich isotherm (Freundlich, 1906) is presented in Eq. (7).

$$q_e = K_F C_e^{1/n} \quad (7)$$

The Freundlich model can be described in the linear form in Eq. (8).

$$\log(q_e) = \log(K_F) + \frac{1}{n} \log(C_e) \quad (8)$$

In the above equation,  $K_F$  (mg<sup>1-1/n</sup> L<sup>1/n</sup> g<sup>-1</sup>) expresses the Freundlich constant, whereas 1/n is used to express the Freundlich constant indicating the strength of the adsorption.

The fittings of the experimental data to isotherm models for MB adsorption by using as-synthesised maghemite nanoparticles are presented in Fig. 14.

Table 5 displays the calculated parameters of adsorption isotherms. Maghemite nanoparticles showed 96.52 mg g<sup>-1</sup> maximum adsorption capacity. Higher values of  $R^2$  showed better fitness of the experimental data of dye removal to the Freundlich isotherm model. This demonstrates the heterogeneous surface of the maghemite adsorbent.

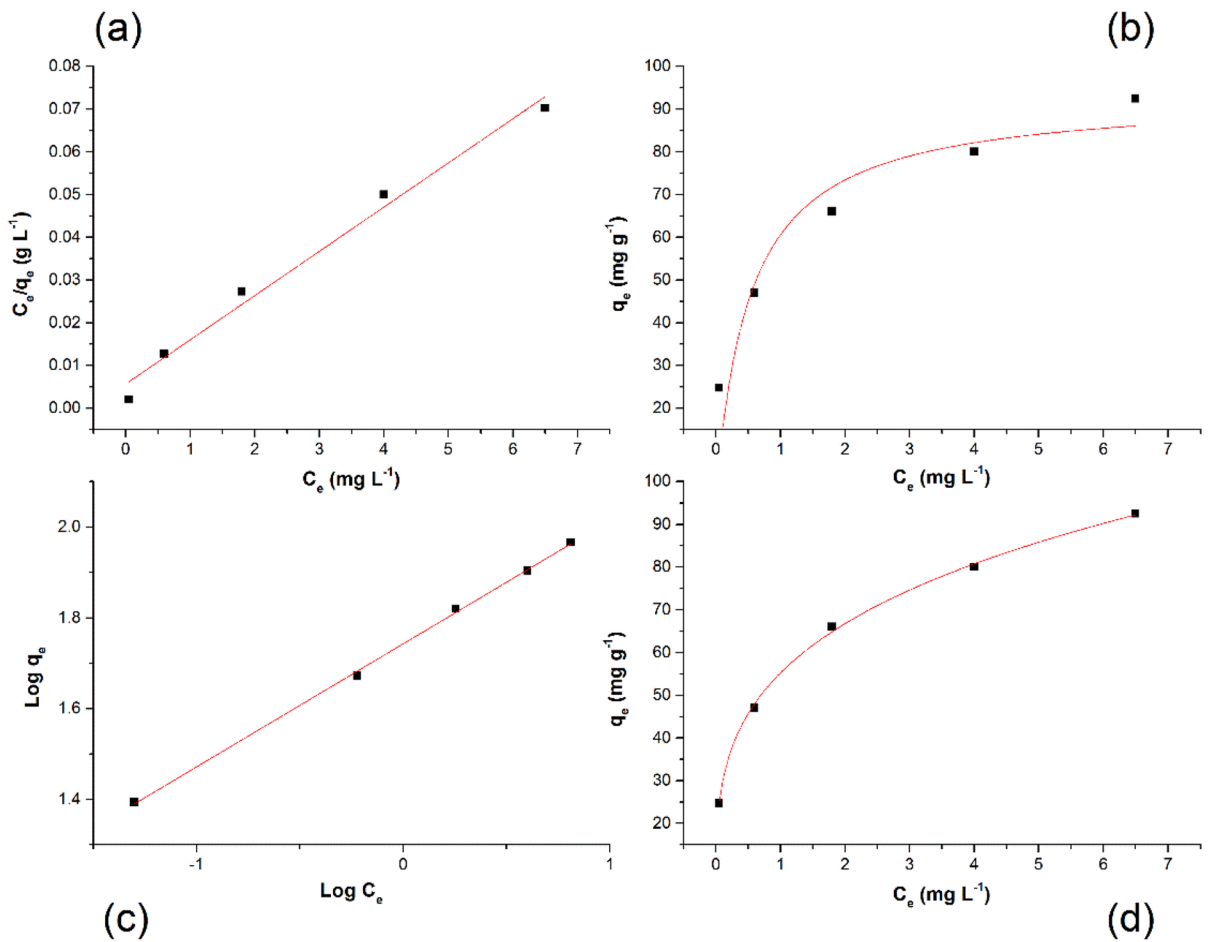


**Fig. 14** Adsorption isotherms models for maghemite nanoparticles: **a** linear Langmuir, **b** nonlinear Langmuir, **c** linear Freundlich, **d** nonlinear Freundlich

**Table 5** Adsorption isotherm parameters for methylene blue

	Langmuir			Freundlich		
	$q_{\max}$ (mg g <sup>-1</sup> )	$K_L$ (L mg <sup>-1</sup> )	$R^2$	$K_F$ (mg <sup>1-1/n</sup> L <sup>1/n</sup> g <sup>-1</sup> )	1/n	$R^2$
Linear	96.52	1.83	0.9861	54.95	0.27	0.9990
Nonlinear	93.15	1.85	0.8728	55.22	0.27	0.9989

Hall et al. (1966) described an important parameter separation factor, “ $R_L$ ”, established on the Langmuir model and is presented in Eq. (9).

$$R_L = \frac{1}{1 + K_L C_o} \tag{9}$$

In the above equation,  $C_0$  expresses the amount of dye at the start of the experiment, and  $K_L$  is used for the Langmuir constant.

$R_L$  explains the feasibility of the adsorption. The types of adsorption were determined by the value of  $R_L$  as follows: linear ( $R_L = 1$ ), favourable ( $0 < R_L < 1$ ), unfavourable ( $R_L > 1$ ), and irreversible ( $R_L = 0$ ).

The calculated  $R_L$  values 0.09 to 0.02 were in between 0 and 1 which confirms that the type of adsorption is favourable for MB on maghemite nanoparticles.

### 3.7.7 Adsorption Kinetics

The kinetics of MB adsorption on maghemite nanoparticles were explored by Lagergren pseudo-first-order and Ho and McKay pseudo-second-order models.

The pseudo-first-order kinetic model (Lagergren, 1898) in nonlinear form is expressed in Eq. (10):

$$q_t = q_e(1 - e^{-K_1 t}) \quad (10)$$

where  $k_1$  ( $\text{min}^{-1}$ ) shows the first-order kinetics' rate constant and  $q_t$  and  $q_e$  ( $\text{mg g}^{-1}$ ) are the amounts adsorbed at any given time  $t$  (min) for adsorbate at equilibrium, respectively.

The pseudo-first-order kinetic model in linear form is written in Eq. (11).

$$\log(q_e - q_t) = \log(q_e) - \frac{K_1 t}{2.303} \quad (11)$$

The pseudo-second-order kinetic model (Ho, 1995, 2006) in nonlinear form is expressed in Eq. (12).

$$q_t = \frac{q_e^2 K_2 t}{(1 + q_e K_2 t)} \quad (12)$$

where  $k_2$  ( $\text{g mg}^{-1} \text{min}^{-1}$ ) shows the rate constant for pseudo-second-order kinetics.

The pseudo-second-order model in its linear form is presented in Eq. (13).

$$\frac{t}{q_t} = \frac{1}{K_2 q_e^2} + \frac{t}{q_e} \quad (13)$$

The adsorption kinetic models of methylene blue by maghemite nanoparticles with linear and

nonlinear regression methods are presented in Fig. 15.

The kinetic parameters and  $R^2$  values for MB adsorption kinetics on maghemite are recorded in Table 6. The values of  $q_e$  and  $K_1$  for the linear form of pseudo-first-order kinetics were estimated from the slope and intercept by drawing the plot between  $\log(q_e - q_t)$  versus time, whereas the slope and intercept form was utilised to calculate the values of  $q_e$  and  $K_2$  for the linear form of pseudo-second-order kinetics by drawing the plot between  $t/q_t$  versus time. The appropriateness of the model was evaluated from the regression coefficient ( $R^2$ ) values. It was observed that the kinetics of MB on maghemite nanoparticles follow a pseudo-second-order kinetic model due to the highest correlation coefficient ( $R^2$ ) values.

### 3.7.8 Adsorption Thermodynamics

Adsorption thermodynamics for methylene blue dye adsorption on maghemite nanoparticles were studied using Eq. (14)

$$\Delta G^\circ = -RT \ln K_c \quad (14)$$

In the above equation,  $\Delta G^\circ$  ( $\text{kJ mol}^{-1}$ ) expresses Gibb's free energy, whereas  $T$  (K) is used for temperature,  $R$  ( $8.314 \text{ J mol}^{-1} \text{ K}^{-1}$ ) is used as a universal gas constant, and  $K_c$  (dimensionless) is the thermodynamic constant.

Equation ((15)) describes the relationship between thermodynamic parameters.

$$\Delta G^\circ = \Delta H^\circ - T \Delta S^\circ \quad (15)$$

In the above equation,  $\Delta H^\circ$  ( $\text{kJ mol}^{-1}$ ) shows the enthalpy of the system, and  $\Delta S^\circ$  ( $\text{J mol}^{-1}$ ) explains the entropy.

The substitution of Eq. (14) into Eq. (15) resulted in the development of the Van't Hoff Eq. (16) which can be stated as follows.

$$\ln K_c = \frac{-\Delta H^\circ}{RT} + \frac{\Delta S^\circ}{R} \quad (16)$$

In the above equation, the value of  $K_c$  can be calculated by multiplying the Langmuir constant by  $10^6$  (Milonjić, 2007, 2009; Tran et al., 2016).  $K_c$  is a dimensionless quantity which is known as a thermodynamic constant.



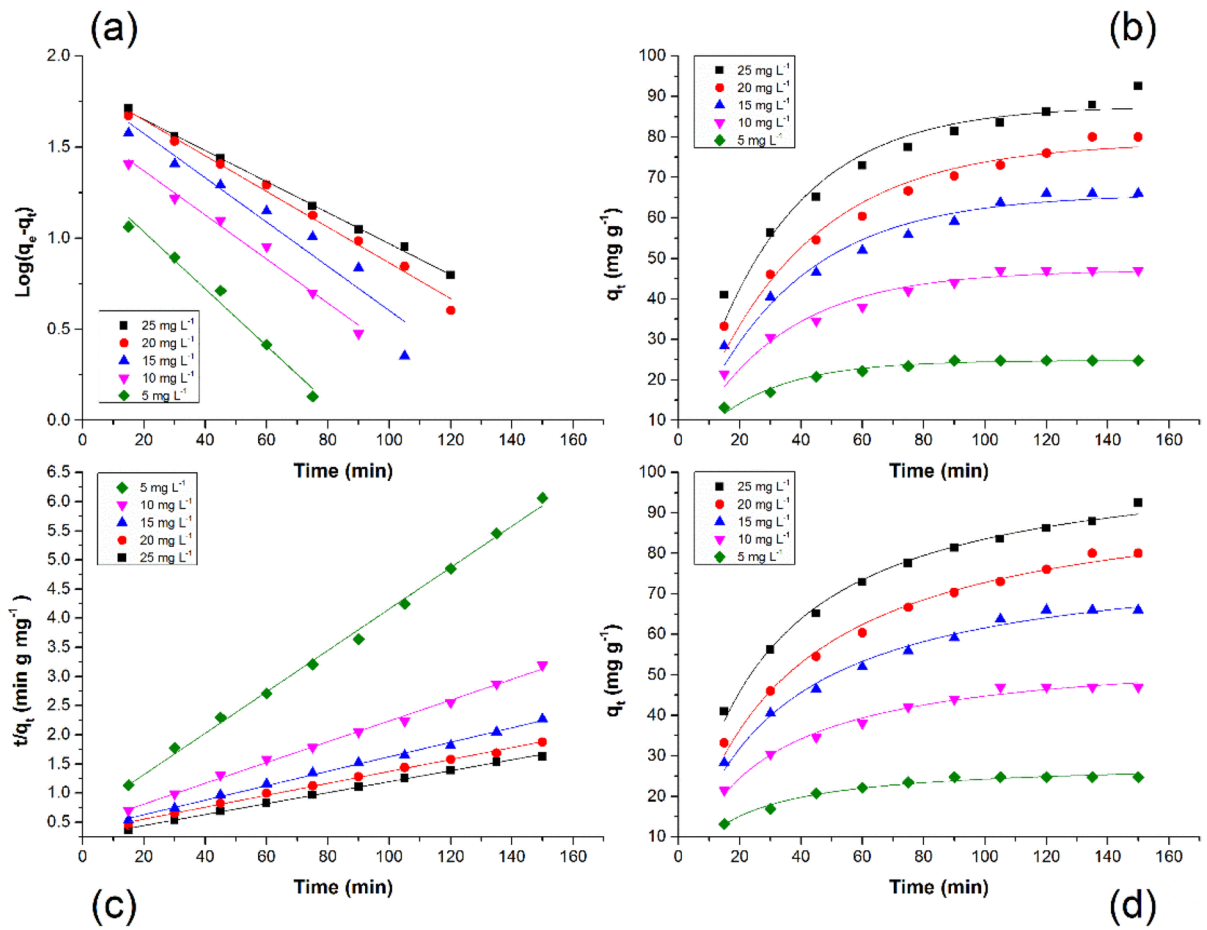


**Fig. 15** MB adsorption kinetics on maghemite: **a** pseudo-first-order linear, **b** pseudo-first-order nonlinear, **c** pseudo-second-order linear, **d** pseudo-second-order nonlinear

**Table 6** MB adsorption kinetic parameters for maghemite nanoparticles

$C_0$ (mg L <sup>-1</sup> )	$q_e, \text{exp}$ (mg g <sup>-1</sup> )	Pseudo first order			Pseudo second order		
		$q_e, \text{cal}$ (mg g <sup>-1</sup> )	$K_1$ (min <sup>-1</sup> )	$R^2$	$q_e, \text{cal}$ (mg g <sup>-1</sup> )	$K_2$ (g mg <sup>-1</sup> min <sup>-1</sup> )	$R^2$
Linear model							
5	24.75	22.19	0.0359	0.9831	28.17	0.0021	0.9966
10	47	40.77	0.0279	0.9843	56.09	0.0007	0.9966
15	66	65.47	0.0279	0.9318	80.58	0.0004	0.9966
20	80	69.71	0.0226	0.9908	97.75	0.0003	0.9970
25	92.50	66.30	0.0196	0.9978	106.38	0.0003	0.9979
Nonlinear model							
5	24.75	24.75	0.0424	0.9703	28.55	0.0020	0.9790
10	47	47.02	0.0329	0.9634	56.35	0.0007	0.9868
15	66	65.83	0.0295	0.9612	80.28	0.0004	0.9887
20	80	78.70	0.0277	0.9613	97.00	0.0003	0.9905
25	92.50	87.66	0.0331	0.9551	105.13	0.0004	0.9924

**Table 7** Important thermodynamic parameters used in adsorption

$T$ (K)	$K_c$	$\Delta G^\circ$ (kJ mol <sup>-1</sup> )	$\Delta H^\circ$ (kJ mol <sup>-1</sup> )	$\Delta S^\circ$ (J mol <sup>-1</sup> )
298	1,830,000	-35.73		
308	1,330,000	-36.11	-19.95	52.37
318	860,000	-36.12		

Equation (14) was used to analyse the amount of  $\Delta G^\circ$ , whereas the slope and intercept form of the plot between  $\ln K_c$  versus  $1/T$ , respectively (Eq. 16), was employed to measure the values of  $\Delta H^\circ$  and  $\Delta S^\circ$ . Thermodynamic parameters are recorded in Table 7 for the adsorption of MB by maghemite nanoparticles. Gibb's free energy ( $\Delta G^\circ$ ) is utilised to calculate the degree of spontaneity for the observed process. Negative  $\Delta G^\circ$  indicates the spontaneous nature of the adsorption of MB on maghemite nanoparticles.

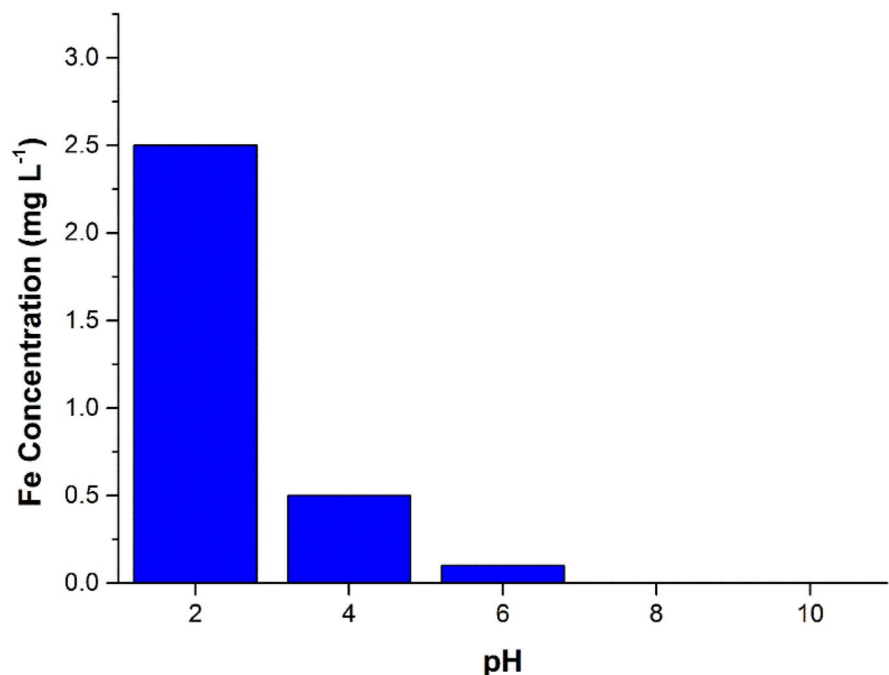
The mechanism of the MB dye removal by maghemite nano-adsorbent is exothermic, which is evident from the negative values of  $\Delta H^\circ$  ( $\Delta H^\circ < 0$ ) as shown in Table 7. This shows that there is a negative correlation between temperature and the equilibrium constant ( $K_c$ ). Further, the positive values of  $\Delta S^\circ$  indicate the random association of the molecules of

dye on maghemite nanoparticles' adsorbent surface. Thermodynamic parameters show that the process is physical adsorption.

### 3.7.9 Adsorbent Stability and Reusability

An adsorbent to be used for wastewater treatment at the industrial level should have good adsorption capacity, be highly stable, and be easily recoverable from the water. Recycling is crucial for reducing the cost of the wastewater treatment process (Hu et al., 2005). The stability of as-synthesised nano-adsorbent was evaluated by leaching test at different pH levels, and outcomes are presented in Fig. 16. Briefly, 0.25-g maghemite nanoparticles were dispersed in 200 mL of water and agitated at 200 rpm for 120 min. At pH 2, the maximum leaching of iron ions was 2.5 mg L<sup>-1</sup> as calculated with atomic absorption spectroscopy and decreased significantly with a rise in solution pH. The negligible results for iron ions leaching were found at pH levels higher than 6, which proves the good stability of the adsorbent at pH values above 6.

The adsorption of MB is maximum at pH level 8 due to higher electrostatic attractions and decreased at lower pH levels. Therefore, the developed adsorbent can be recycled by varying the solution pH. To analyse the reusability and recycling of maghemite

**Fig. 16** Iron ions leaching results at various pH levels

**Fig. 17** Percentage of dye removal performance after ten reuse cycles for maghemite nanoparticles

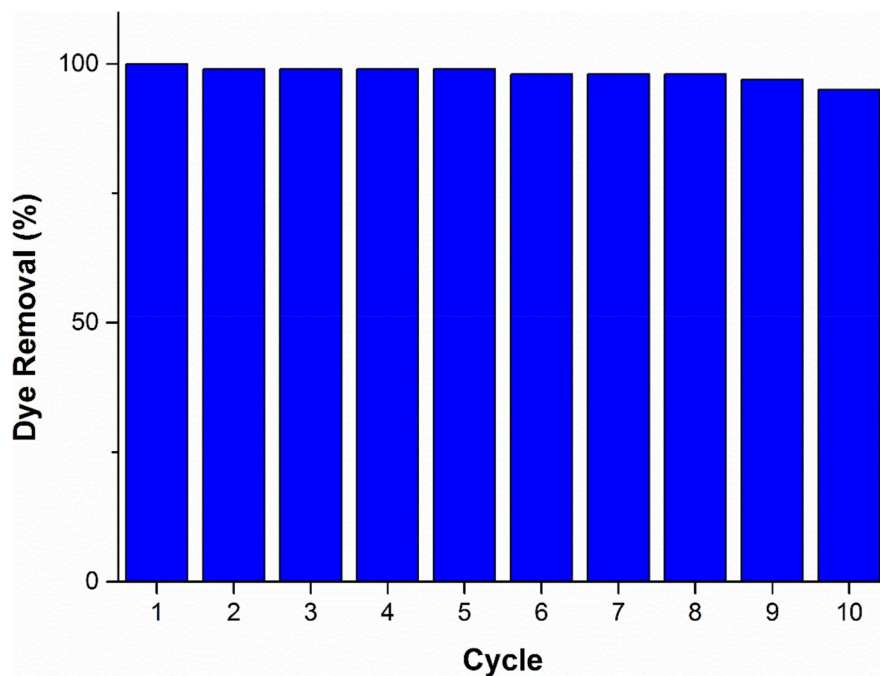


**Table 8** Comparative adsorption performance of different materials for MB dye

Adsorbent	$q_m$ (mg g <sup>-1</sup> )	References
Iron oxide-coated zeolite	18.6	Zhao et al. (2010)
MWCNT	15.87	Gong et al. (2009)
Iron-impregnated AC	20.61	Naeem et al. (2016)
Activated carbon from coir	3.53	de Souza Macedo et al. (2006)
Bagasse fly ash	2.26	Aygün et al. (2003)
MnP	25.54	Păcurariu et al. (2016)
Magnetised bentonite	39.54	Lou et al. (2015)
Fe <sub>3</sub> O <sub>4</sub> @C	44.38	Zhang et al. (2011)
Acrylic waste	8.76	Naeem et al. (2017)
Maghemite nanoparticles	96.52	This work

nanoparticles, the adsorption and desorption were performed for ten cycles. The results are shown in Fig. 17. Maghemite nanoparticles exhibit 95% dye removal efficiency even after ten cycles, which shows excellent recycling performance.

### 3.7.10 Comparison of Maghemite Adsorbent for the Removal of MB with Other Adsorbents

For practical uses and economic considerations, it is critical to compare the effectiveness of various adsorbents for the elimination of pollutants.

Therefore, the comparison of the synthesised maghemite nanoparticles with many other materials for the elimination of methylene blue dye has been presented in Table 8. The adsorption capacity (96.52 mg g<sup>-1</sup>) of maghemite nanoparticles obtained from the Langmuir isotherm is better than that of many adsorbents for removing dyes from water, as mentioned in Table 8, which shows their good potential for efficient wastewater treatment. The higher adsorption capacity of maghemite nanoparticles is attributed to the higher surface area of the nanoparticles.

## 4 Conclusions

In this study, an efficient and economical method was developed to prepare maghemite nanoparticles by an ultrasonic-assisted modified co-precipitation technique. Nanoparticle size can be controlled systematically with adjustments to the processing conditions. Iron oxide nanoparticles have been fabricated by an economical and environment-friendly method without using any surfactant or solvent, which shows the large-scale production potential of pure iron oxide nanoparticles. The effect of process variables was modelled and analysed with Box–Behnken statistical design and response surface methodology using Design-Expert software. The best outcome with 25-nm size was achieved with optimum processing conditions at a pH level of 12, a temperature of 70 °C, and a time of 60 min. The prepared maghemite nanoparticles were successfully employed for the adsorption of MB dye from water. The maximum adsorption capacity of maghemite nanoparticles was observed to be 96.52 mg g<sup>-1</sup>.

From the studies for the comparison of the adsorption capacity of the synthesised nanoparticles with other materials in the same field, it was suggested that the maghemite nanoparticles are of greater interest. Higher values of  $R^2$  showed better fitness of the experimental data on dye removal to the Freundlich isotherm model and pseudo-second-order kinetic model. Maghemite nanoparticles can be easily restored and reused repeatedly, as observed from desorption studies, so they can facilitate dye removal in textile industries. The easy synthesis method, good adsorption capacity, and simple magnetic recovery of these maghemite nanoparticles make these particles excellent adsorbents. Although maghemite nanoparticles have been found to be excellent adsorbents for the elimination of dyes, the adsorption process is still the subject of more specialised wastewater treatment analyses. On the other hand, the development of novel effective systems for the treatment of wastewater containing multiple contaminants could be an interesting innovation for the future.

**Data Availability** Data are available on request from the authors.

## Declarations

**Conflict of Interest** The authors declare no competing interests.

## References

- Abrouki, Y., Mabrouki, J., Anouzla, A., Rifi, S. K., Zahiri, Y., Nehhal, S., & Souabi, S. (2021). Optimization and modeling of a fixed-bed biosorption of textile dye using agricultural biomass from the Moroccan Sahara. *Desalination and Water Treatment*, 240, 144–151.
- Al-Degs, Y., Khraisheh, M., Allen, S., & Ahmad, M. (2000). Effect of carbon surface chemistry on the removal of reactive dyes from textile effluent. *Water Research*, 34(3), 927–935.
- Al-Ghouti, M., Khraisheh, M., Allen, S., & Ahmad, M. (2003). The removal of dyes from textile wastewater: A study of the physical characteristics and adsorption mechanisms of diatomaceous earth. *Journal of Environmental Management*, 69(3), 229–238.
- Anouzla, A., Abrouki, Y., Souabi, S., Safi, M., & Rhal, H. (2009). Colour and COD removal of disperse dye solution by a novel coagulant: Application of statistical design for the optimization and regression analysis. *Journal of Hazardous Materials*, 166(2–3), 1302–1306.
- Anouzla, A., Kastali, M., Azoulay, K., Bencheikh, I., Fattah, G., Mabrouki, J., . . . & Bakkouche, C. (2022). Multi-response optimization of coagulation–flocculation process for stabilized landfill leachate treatment using a coagulant based on an industrial effluent. *Desalination and Water Treatment*, 254, 71–79. <https://doi.org/10.5004/dwt.2022.28388>
- Aygün, A., Yenisoy-Karakaş, S., & Duman, I. (2003). Production of granular activated carbon from fruit stones and nutshells and evaluation of their physical, chemical and adsorption properties. *Microporous and Mesoporous Materials*, 66(2), 189–195.
- Azarang, M., Shuhaimi, A., Yousefi, R., Golsheikh, A. M., & Sookhakian, M. (2014). Synthesis and characterization of ZnO NPs/reduced graphene oxide nanocomposite prepared in gelatin medium as highly efficient photo-degradation of MB. *Ceramics International*, 40(7), 10217–10221.
- Azarang, M., Shuhaimi, A., Yousefi, R., & Jahromi, S. P. (2015). One-pot sol–gel synthesis of reduced graphene oxide uniformly decorated zinc oxide nanoparticles in starch environment for highly efficient photodegradation of methylene blue. *RSC Advances*, 5(28), 21888–21896.
- Binh, V. T., Purcell, S., Semet, V., & Feschet, F. (1998). Nanotips and nanomagnetism. *Applied Surface Science*, 130, 803–814.
- Cao, M., Liu, T., Gao, S., Sun, G., Wu, X., Hu, C., & Wang, Z. L. (2005). Single-crystal dendritic micro-pines of magnetic  $\alpha$ -Fe<sub>2</sub>O<sub>3</sub>: Large-scale synthesis, formation mechanism, and properties. *Angewandte Chemie International Edition*, 44(27), 4197–4201.
- Chauhan, P., Annapoorni, S., & Trikha, S. (1999). Humidity-sensing properties of nanocrystalline haematite thin films prepared by sol-gel processing. *Thin Solid Films*, 346(1), 266–268.

- de Souza Macedo, J., da Costa Júnior, N. B., Almeida, L. E., da Silva Vieira, E. F., Cestari, A. R., de Fátima Gimenez, I., . . . Barreto, L. S. (2006). Kinetic and calorimetric study of the adsorption of dyes on mesoporous activated carbon prepared from coconut coir dust. *Journal of Colloid and Interface Science*, 298(2), 515–522.
- Espantaleon, A., Nieto, J., Fernandez, M., & Marsal, A. (2003). Use of activated clays in the removal of dyes and surfactants from tannery waste waters. *Applied Clay Science*, 24(1–2), 105–110.
- Fernandez, J., Kiwi, J., Lizama, C., Freer, J., Baeza, J., & Mansilla, H. (2002). Factorial experimental design of Orange II photocatalytic discoloration. *Journal of Photochemistry and Photobiology a: Chemistry*, 151(1–3), 213–219.
- Ferrero, F. (2015). Dye removal from aqueous solution using coal fly ash for continuous flow adsorption. *Clean Technologies and Environmental Policy*, 17(7), 1907–1915.
- Freundlich, H. (1906). Über die adsorption in lasugen. *Journal of Physical Chemistry*, 57, 385–470.
- Ganguli, A. K., & Ahmad, T. (2007). Nanorods of iron oxalate synthesised using reverse micelles: Facile route for  $\alpha$ -Fe<sub>2</sub>O<sub>3</sub> and Fe<sub>3</sub>O<sub>4</sub> nanoparticles. *Journal of Nanoscience and Nanotechnology*, 7(6), 2029–2035.
- Garcell, L., Morales, M. P., Andres-Verges, M., Tartaj, P., & Serna, C. J. (1998). Interfacial and rheological characteristics of maghemite aqueous suspensions. *Journal of Colloid and Interface Science*, 205(2), 470–475. <https://doi.org/10.1006/jcis.1998.5654>
- Gedanken, A. (2004). Using sonochemistry for the fabrication of nanomaterials. *Ultrasonics Sonochemistry*, 11(2), 47–55.
- Ghows, N., & Entezari, M. H. (2010). Ultrasound with low intensity assisted the synthesis of nanocrystalline TiO<sub>2</sub> without calcination. *Ultrasonics Sonochemistry*, 17(5), 878–883.
- Giri, S., Das, N., & Pradhan, G. (2011). Synthesis and characterization of magnetite nanoparticles using waste iron ore tailings for adsorptive removal of dyes from aqueous solution. *Colloids and Surfaces a: Physicochemical and Engineering Aspects*, 389(1), 43–49.
- Gong, J.-L., Wang, B., Zeng, G.-M., Yang, C.-P., Niu, C.-G., Niu, Q.-Y., . . . Liang, Y. (2009). Removal of cationic dyes from aqueous solution using magnetic multi-wall carbon nanotube nanocomposite as adsorbent. *Journal of Hazardous materials*, 164(2), 1517–1522.
- Goss, C. (1988). Saturation magnetisation, coercivity and lattice parameter changes in the system Fe<sub>3</sub>O<sub>4</sub>- $\gamma$ -Fe<sub>2</sub>O<sub>3</sub>, and their relationship to structure. *Physics and Chemistry of Minerals*, 16(2), 164–171.
- Guivar, J. A. R., Martínez, A. I., Anaya, A. O., Valladares, L. D. L. S., Félix, L. L., & Dominguez, A. B. (2014). Structural and magnetic properties of monophasic maghemite ( $\gamma$ -Fe<sub>2</sub>O<sub>3</sub>) nanocrystalline powder. *Advances in Nanoparticles*, 3(3), 114–121.
- Guo, J., Zhu, S., Chen, Z., Li, Y., Yu, Z., Liu, Q., . . . & Zhang, D. (2011). Sonochemical synthesis of TiO<sub>2</sub> nanoparticles on graphene for use as photocatalyst. *Ultrasonics Sonochemistry*, 18(5), 1082–1090.
- Hall, K. R., Eagleton, L. C., Acrivos, A., & Vermeulen, T. (1966). Pore-and solid-diffusion kinetics in fixed-bed adsorption under constant-pattern conditions. *Industrial & Engineering Chemistry Fundamentals*, 5(2), 212–223.
- Ho, Y.-S. (1995). *Adsorption of heavy metals from waste streams by peat*. Ph. D. Thesis, The University of Bringham. <https://etheses.bham.ac.uk/id/eprint/8742/>
- Ho, Y.-S. (2006). Second-order kinetic model for the sorption of cadmium onto tree fern: A comparison of linear and non-linear methods. *Water Research*, 40(1), 119–125.
- Horner, O., Neveu, S., de Montredon, S., Siaugue, J.-M., & Cabuil, V. (2009). Hydrothermal synthesis of large maghemite nanoparticles: Influence of the pH on the particle size. *Journal of Nanoparticle Research*, 11(5), 1247–1250.
- Hu, J., Chen, G., & Lo, I. M. (2005). Removal and recovery of Cr (VI) from wastewater by maghemite nanoparticles. *Water Research*, 39(18), 4528–4536.
- Hyeon, T., Lee, S. S., Park, J., Chung, Y., & Na, H. B. (2001). Synthesis of highly crystalline and monodisperse maghemite nanocrystallites without a size-selection process. *Journal of the American Chemical Society*, 123(51), 12798–12801.
- Imran, M., Khan, Z. U. H., Iqbal, M. M., Iqbal, J., Shah, N. S., Munawar, S., . . . & Rizwan, M. (2020). Effect of bio-char modified with magnetite nanoparticles and HNO<sub>3</sub> for efficient removal of Cr (VI) from contaminated water: A batch and column scale study. *Environmental Pollution*, 261, 114231.
- Iqbal, J., Shah, N. S., Sayed, M., Imran, M., Muhammad, N., Howari, F. M., . . . Bhatnagar, A. (2019). Synergistic effects of activated carbon and nano-zerovalent copper on the performance of hydroxyapatite-alginate beads for the removal of As<sub>3+</sub> from aqueous solution. *Journal of Cleaner Production*, 235, 875–886.
- Jing, Z. (2006). Preparation and magnetic properties of fibrous gamma iron oxide nanoparticles via a nonaqueous medium. *Materials Letters*, 60(17), 2217–2221.
- Kosmulski, M. (2009). *Surface charging and points of zero charge* (1st ed., p. 1092). CRC Press. <https://doi.org/10.1201/9781420051896>
- Kumar, K. V., & Kumaran, A. (2005). Removal of methylene blue by mango seed kernel powder. *Biochemical Engineering Journal*, 27(1), 83–93.
- Lagergren, S. (1898). Zur theorie der sogenannten adsorption gelöster stoffe. *Kungliga Svenska Vetenskapsakademiens Handlingar*, 24(4), 1–39.
- Langmuir, I. (1916). The constitution and fundamental properties of solids and liquids. Part I. Solids. *Journal of the American Chemical Society*, 38(11), 2221–2295. [https://scholar.archive.org/work/jzbfns3bvnfvvpmr7uluelkypi/access/ia\\_file/crossref-pre-1923-scholarly-works/10.1021%252Fja02267a023.zip/10.1021%252Fja02268a002.pdf](https://scholar.archive.org/work/jzbfns3bvnfvvpmr7uluelkypi/access/ia_file/crossref-pre-1923-scholarly-works/10.1021%252Fja02267a023.zip/10.1021%252Fja02268a002.pdf)
- Lee, C.-K., Liu, S.-S., Juang, L.-C., Wang, C.-C., Lin, K.-S., & Lyu, M.-D. (2007). Application of MCM-41 for dyes removal from wastewater. *Journal of Hazardous Materials*, 147(3), 997–1005.
- Lee, J.-W., Choi, S.-P., Thiruvengatachari, R., Shim, W.-G., & Moon, H. (2006). Submerged microfiltration membrane coupled with alum coagulation/powdered activated carbon adsorption for complete decolorization of reactive dyes. *Water Research*, 40(3), 435–444.
- Lou, Z., Zhou, Z., Zhang, W., Zhang, X., Hu, X., Liu, P., & Zhang, H. (2015). Magnetized bentonite by Fe<sub>3</sub>O<sub>4</sub>

- nanoparticles treated as adsorbent for methylene blue removal from aqueous solution: Synthesis, characterization, mechanism, kinetics and regeneration. *Journal of the Taiwan Institute of Chemical Engineers*, 49, 199–205.
- Loukili, H., Alami-Younsi, S., Albizane, A., Bennazha, J., Bouhria, M., Persin, M., & Larbot, A. (2008). Investigation of performance of a low ZnAl<sub>2</sub>O<sub>4</sub>-TiO<sub>2</sub> ultrafiltration membrane in relation with speciation and membrane solutes interactions. *Separation and Purification Technology*, 59(2), 134–140.
- Loukilia, H., Mabroukic, J., Anouzlab, A., Kouzia, Y., Younssia, S. A., Diguab, K., & Abroukic, Y. (2021). Pre-treated Moroccan natural clays: Application to the wastewater treatment of textile industry. *Desalination Water Treat*, 240, 124–136.
- Mahanta, D., Madras, G., Radhakrishnan, S., & Patil, S. (2008). Adsorption of sulfonated dyes by polyaniline emeraldine salt and its kinetics. *The Journal of Physical Chemistry B*, 112(33), 10153–10157.
- Mendoza, M., Donado, F., Silva, R., Pérez, M., & Carrillo, J. (2005). Magnetite microcrystals for magneto-rheological fluids. *Journal of Physics and Chemistry of Solids*, 66(6), 927–931.
- Milonjić, S. K. (2007). A consideration of the correct calculation of thermodynamic parameters of adsorption. *Journal of the Serbian Chemical Society*, 72(12), 1363–1367.
- Milonjić, S. K. (2009). Comments on “removal of uranium (VI) from aqueous solution by adsorption of hematite”, by X. Shuibo, Z. Chun, Z. Xinghuo, Y. Jing, Z. Xiaojian, W. Jingsong. *Journal of Environmental Radioactivity*, 10(100), 921–922.
- Morales, M., Veintemillas-Verdaguer, S., Montero, M., Serna, C., Roig, A., Casas, L., . . . & Sandiumenge, F. (1999). Surface and internal spin canting in  $\gamma$ -Fe<sub>2</sub>O<sub>3</sub> nanoparticles. *Chemistry of Materials*, 11(11), 3058–3064.
- Morello, A. P., III., Burrill, R., & Mathiowitz, E. (2007). Preparation and characterization of poly (methyl methacrylate)—iron (III) oxide microparticles using a modified solvent evaporation method. *Journal of Microencapsulation*, 24(5), 476–491.
- Moussadik, A., Lazar, N.-e., Mazkad, D., Brigiano, F. S., Baert, K., Hauffman, T., . . . Tielens, F. (2023). Investigation of electronic and photocatalytic properties of AgTi<sub>2</sub>(PO<sub>4</sub>)<sub>3</sub> NASICON-type phosphate: Combining experimental data and DFT calculations. *Journal of Photochemistry and Photobiology A: Chemistry*, 435, 114289.
- Naeem, M. A., Imran, M., Amjad, M., Abbas, G., Tahir, M., Murtaza, B., . . . Ahmad, I. (2019). Batch and column scale removal of cadmium from water using raw and acid activated wheat straw biochar. *Water*, 11(7), 1438.
- Naeem, S., Baheti, V., Militky, J., Wiener, J., Behera, P., & Ashraf, A. (2016). Sorption properties of iron impregnated activated carbon web for removal of methylene blue from aqueous media. *Fibers and Polymers*, 17(8), 1245–1255.
- Naeem, S., Baheti, V., Wiener, J., & Marek, J. (2017). Removal of methylene blue from aqueous media using activated carbon web. *Journal of the Textile Institute*, 108(5), 803–811.
- Nguyen, H. Q. V., Nerut, J., Kasuk, H., Thomberg, T., Romann, T., Aruväli, J., & Lust, E. (2023). Ultra-small ceria nanocrystals at carbon surface synthesised by ultrasound sonication: A study of highly active platinum-cerium bifunctional catalysts for methanol oxidation and oxygen reduction. *ECS Transactions*, 111(5), 17.
- Noman, M. T., Petru, M., Militký, J., Azeem, M., & Ashraf, M. A. (2019). One-pot sonochemical synthesis of ZnO nanoparticles for photocatalytic applications, modelling and optimization. *Materials*, 13(1), 14.
- Păcurariu, C., Paşka, O., Ianoş, R., & Muntean, S. G. (2016). Effective removal of methylene blue from aqueous solution using a new magnetic iron oxide nanosorbent prepared by combustion synthesis. *Clean Technologies and Environmental Policy*, 18(3), 705–715.
- Patil, M. N., & Pandit, A. B. (2007). Cavitation—a novel technique for making stable nano-suspensions. *Ultrasonics Sonochemistry*, 14(5), 519–530.
- Rachiq, T., Abrouki, Y., Mabrouki, J., Samghouli, N., Fersib, C., Rahal, S., & El Hajjaji, S. (2021). Evaluation of the efficiency of different materials to remove specific pollutants from landfill leachate. *Desalination Water Treat*, 238, 240–250.
- Raming, T., Winnubst, A., van Kats, C. M., & Philipse, A. (2002). The synthesis and magnetic properties of nano-sized hematite ( $\alpha$ -Fe<sub>2</sub>O<sub>3</sub>) particles. *Journal of Colloid and Interface Science*, 249(2), 346–350.
- Rockenberger, J., Scher, E. C., & Alivisatos, A. P. (1999). A new nonhydrolytic single-precursor approach to surfactant-capped nanocrystals of transition metal oxides. *Journal of the American Chemical Society*, 121(49), 11595–11596.
- Saravanan, P., Hsu, J.-H., Sivaprahasam, D., & Kamat, S. (2013). Structural and magnetic properties of  $\gamma$ -Fe<sub>2</sub>O<sub>3</sub> nanostructured compacts processed by spark plasma sintering. *Journal of Magnetism and Magnetic Materials*, 346, 175–177.
- Shi, B., Li, G., Wang, D., Feng, C., & Tang, H. (2007). Removal of direct dyes by coagulation: The performance of preformed polymeric aluminum species. *Journal of Hazardous Materials*, 143(1–2), 567–574.
- Sonavane, S. U., Gawande, M. B., Deshpande, S. S., Venkataraman, A., & Jayaram, R. V. (2007). Chemoselective transfer hydrogenation reactions over nanosized  $\gamma$ -Fe<sub>2</sub>O<sub>3</sub> catalyst prepared by novel combustion route. *Catalysis Communications*, 8(11), 1803–1806.
- Tran, H. N., You, S.-J., & Chao, H.-P. (2016). Thermodynamic parameters of cadmium adsorption onto orange peel calculated from various methods: A comparison study. *Journal of Environmental Chemical Engineering*, 4(3), 2671–2682.
- Uddin, M. T., Islam, M. A., Mahmud, S., & Rukanuzzaman, M. (2009). Adsorptive removal of methylene blue by tea waste. *Journal of Hazardous Materials*, 164(1), 53–60.
- Vayssieres, L. (2009). On the effect of nanoparticle size on water-oxide interfacial chemistry. *Journal of Physical Chemistry C*, 113(12), 4733–4736. <https://doi.org/10.1021/jp810721f>
- Woo, K., Hong, J., Choi, S., Lee, H.-W., Ahn, J.-P., Kim, C. S., & Lee, S. W. (2004). Easy synthesis and magnetic properties of iron oxide nanoparticles. *Chemistry of Materials*, 16(14), 2814–2818.

- Wu, W., He, Q., & Jiang, C. (2008). Magnetic iron oxide nanoparticles: Synthesis and surface functionalization strategies. *Nanoscale Research Letters*, 3(11), 397–415.
- Wu, W., Xiao, X., Zhang, S., Peng, T., Zhou, J., Ren, F., & Jiang, C. (2010). Synthesis and magnetic properties of maghemite ( $\gamma\text{-Fe}_2\text{O}_3$ ) short-nanotubes. *Nanoscale Research Letters*, 5(9), 1474.
- Yousefi, R., Jamali-Sheini, F., Cheraghizade, M., Khosravi-Gandomani, S., Saaedi, A., Huang, N. M., . . . Azarang, M. (2015). Enhanced visible-light photocatalytic activity of strontium-doped zinc oxide nanoparticles. *Materials Science in Semiconductor Processing*, 32, 152–159.
- Yu, Y., Zhuang, Y.-Y., Wang, Z.-H., & Qiu, M.-Q. (2003). Adsorption of water-soluble dyes onto resin NKZ. *Industrial & Engineering Chemistry Research*, 42(26), 6898–6903.
- Zhang, W., Liang, F., Li, C., Qiu, L.-G., Yuan, Y.-P., Peng, F.-M., . . . Zhu, J.-F. (2011). Microwave-enhanced synthesis of magnetic porous covalent triazine-based framework composites for fast separation of organic dye from aqueous solution. *Journal of Hazardous materials*, 186(2), 984–990.
- Zhang W, Metzger H, Vlatakis S, Claxton A, Carbajal M, A, Fung L. F., . . . Fleck, R. A. (2023). Characterising the chemical and physical properties of phase-change nanodroplets. *Ultrasonics Sonochemistry*, 106445.
- Zhao, L., Zou, W., Zou, L., He, X., Song, J., & Han, R. (2010). Adsorption of methylene blue and methyl orange from aqueous solution by iron oxide-coated zeolite in fixed bed column: Predicted curves. *Desalination and Water Treatment*, 22(1–3), 258–264.
- Zhao R, Li X, Li Y, Li Y, Sun B, Zhang N, . . . Wang, C. (2017). Functionalized magnetic iron oxide/polyacrylonitrile composite electrospun fibers as effective chromium (VI) adsorbents for water purification. *Journal of Colloid and Interface Science*, 505, 1018–1030.
- Zhao, R., Li, X., Sun, B., Li, Y., Li, Y., & Wang, C. (2017b). Preparation of molecularly imprinted sericin/poly (vinyl alcohol) electrospun fibers for selective removal of methylene blue. *Chemical Research in Chinese Universities*, 33(6), 986–994.
- Zhao, R., Wang, Y., Li, X., Sun, B., & Wang, C. (2015). Synthesis of  $\beta$ -cyclodextrin-based electrospun nanofiber membranes for highly efficient adsorption and separation of methylene blue. *ACS Applied Materials & Interfaces*, 7(48), 26649–26657.
- Zhong, L. S., Hu, J. S., Liang, H. P., Cao, A. M., Song, W. G., & Wan, L. J. (2006). Self-Assembled 3D flowerlike iron oxide nanostructures and their application in water treatment. *Advanced Materials*, 18(18), 2426–2431.
- Zhou, L., Gao, C., & Xu, W. (2010). Magnetic dendritic materials for highly efficient adsorption of dyes and drugs. *ACS Applied Materials & Interfaces*, 2(5), 1483–1491.

**Publisher's Note** Springer Nature remains neutral with regard to jurisdictional claims in published maps and institutional affiliations.

Springer Nature or its licensor (e.g. a society or other partner) holds exclusive rights to this article under a publishing agreement with the author(s) or other rightsholder(s); author self-archiving of the accepted manuscript version of this article is solely governed by the terms of such publishing agreement and applicable law.